Single heteroatom fine tuning of the emissive properties in organoboron complexes with 7-(azaheteroaryl)indole systems.

Miriam Más-Montoya, Laura Usea, Arturo Espinosa Ferao, María F. Montenegro, Carmen Ramírez de Arellano, Alberto Tárraga, José N. Rodríguez-López and David Curiel*.

SUPPORTING INFORMATION

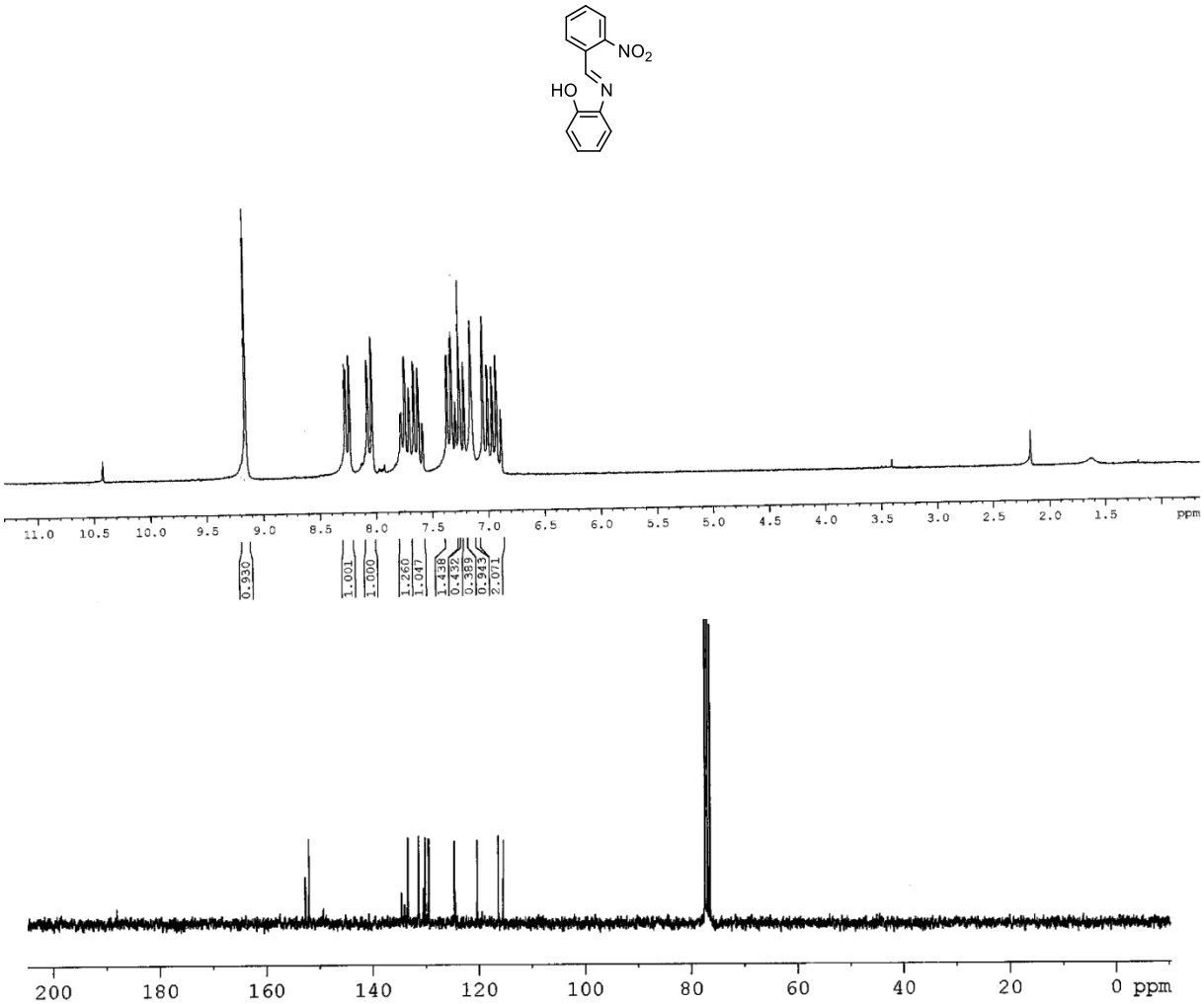

Figure S1. ^{1}H-NMR and ^{13}C-NMR spectra of compound **1**.

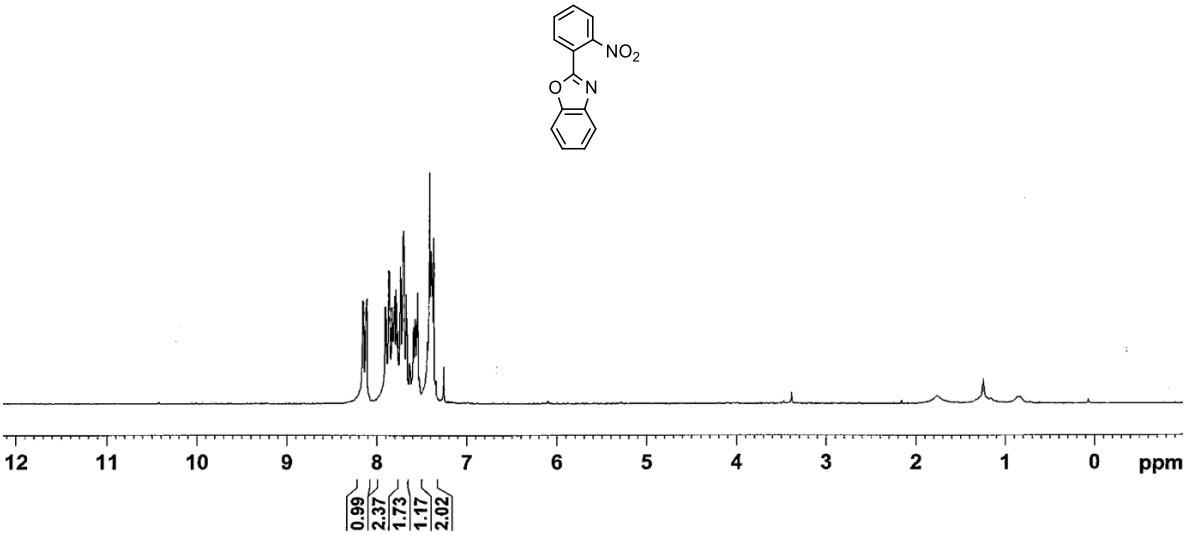

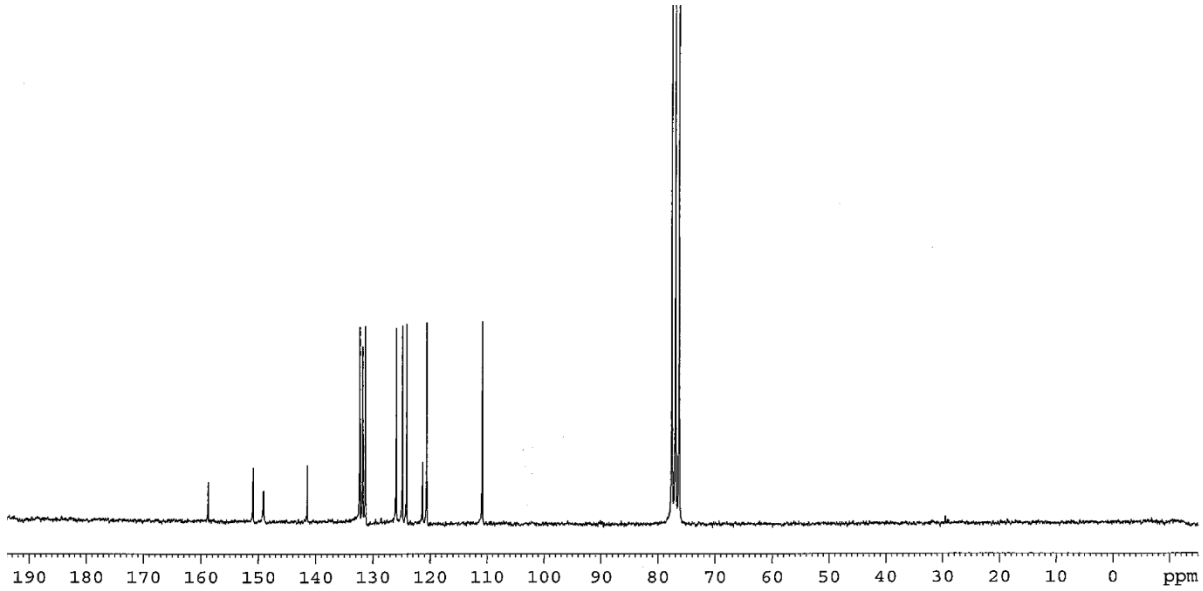

Figure S2. ^{1}H-NMR and ^{13}C-NMR spectra of compound **2**.

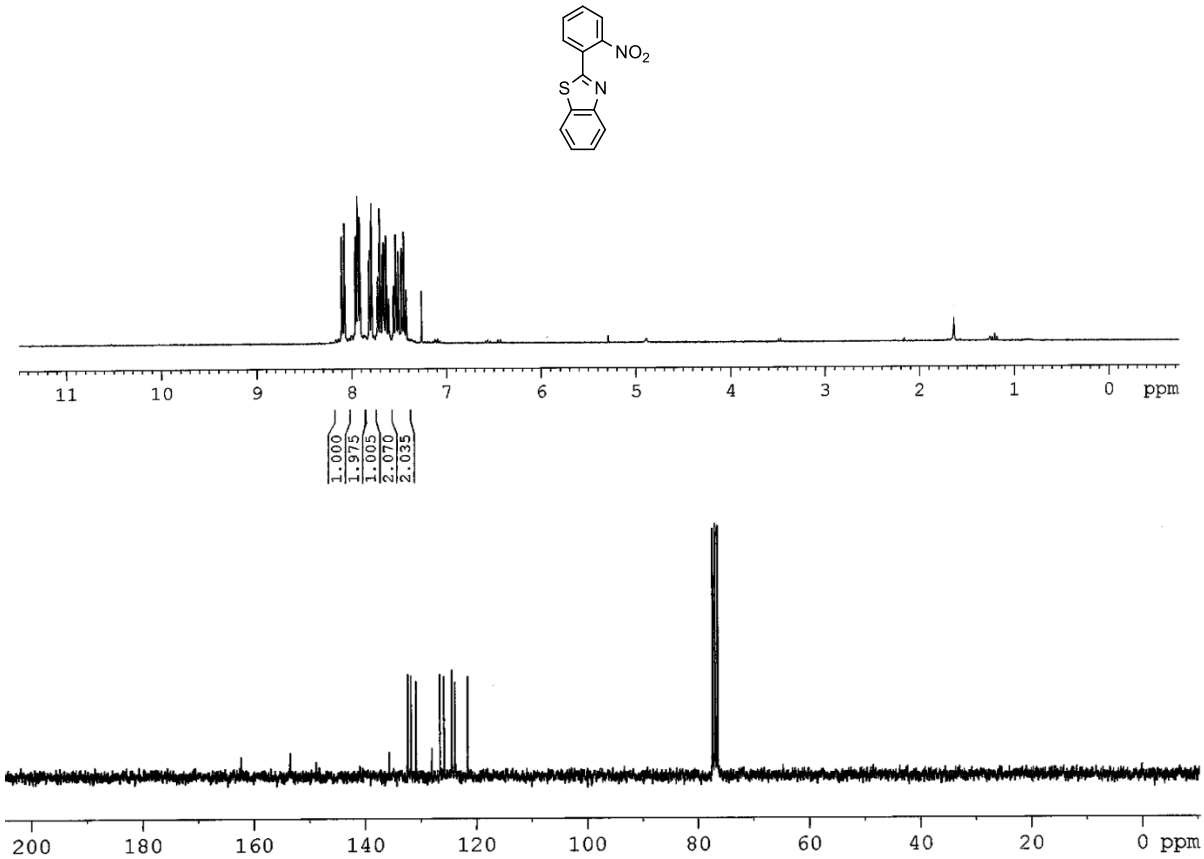

Figure S3. ^{1}H-NMR and ^{13}C-NMR spectra of compound **3**.

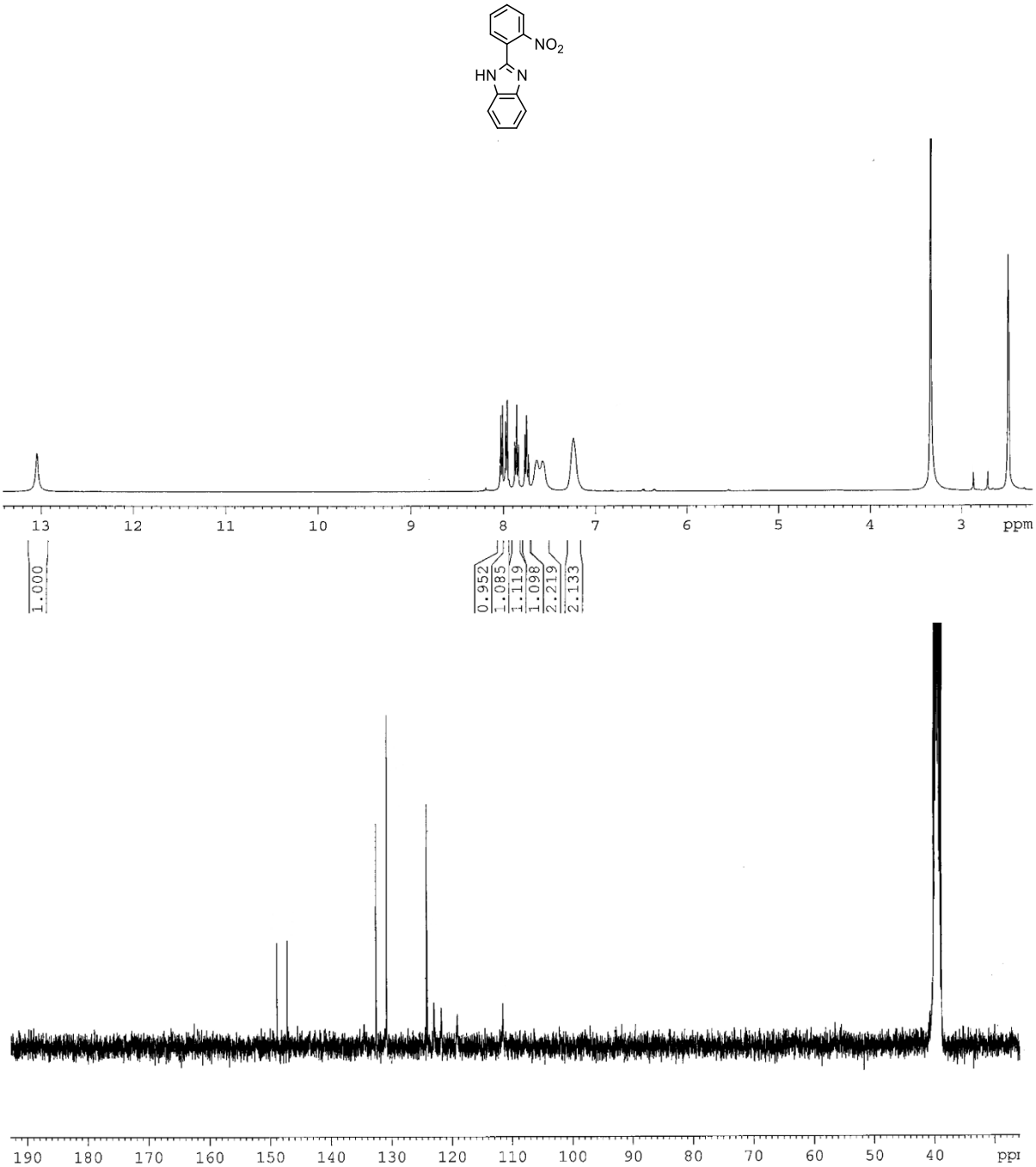

Figure S4. ^{1}H-NMR and ^{13}C-NMR spectra of compound **4**

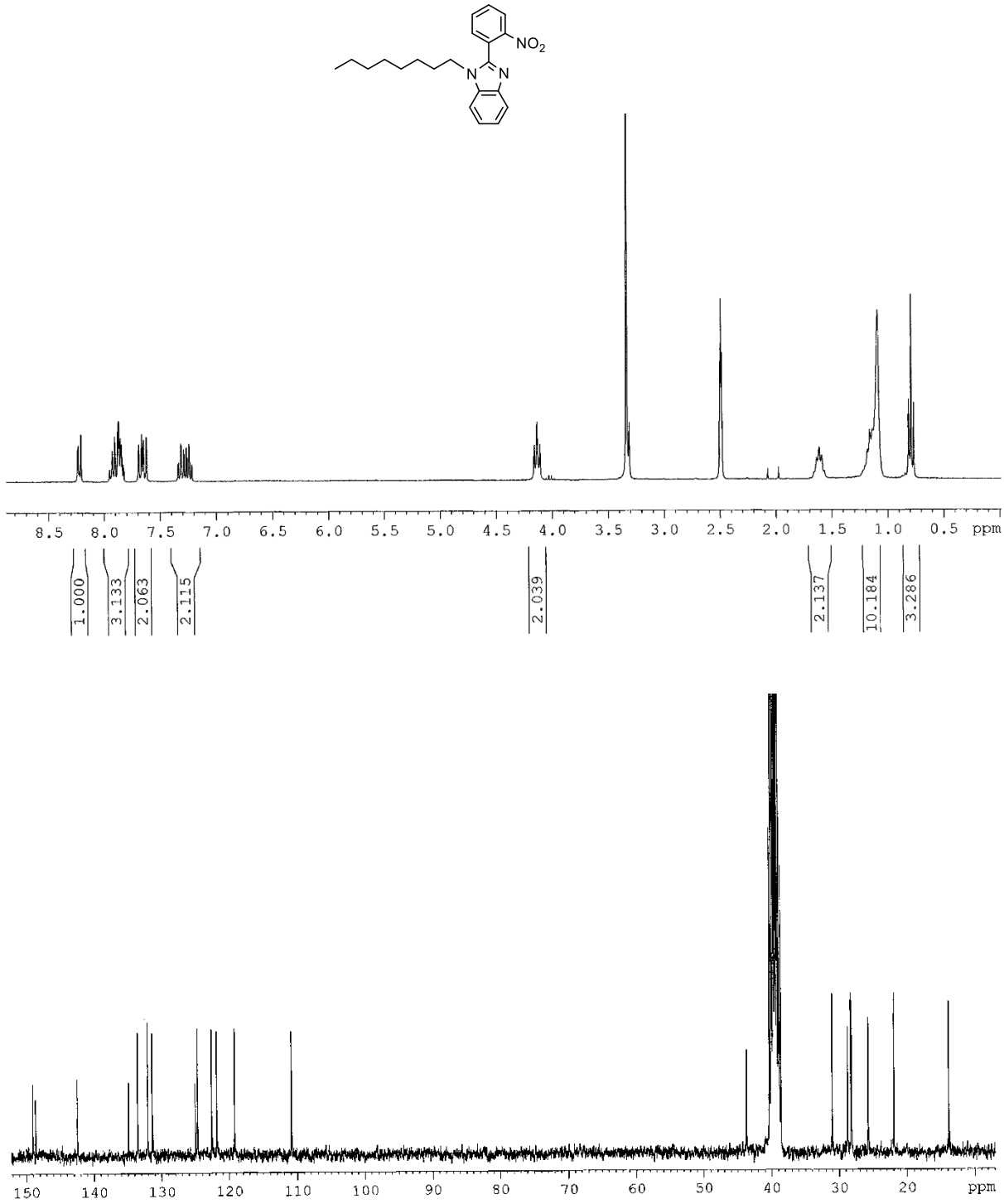

Figure S5. ^{1}H-NMR and ^{13}C-NMR spectra of compound **5**.

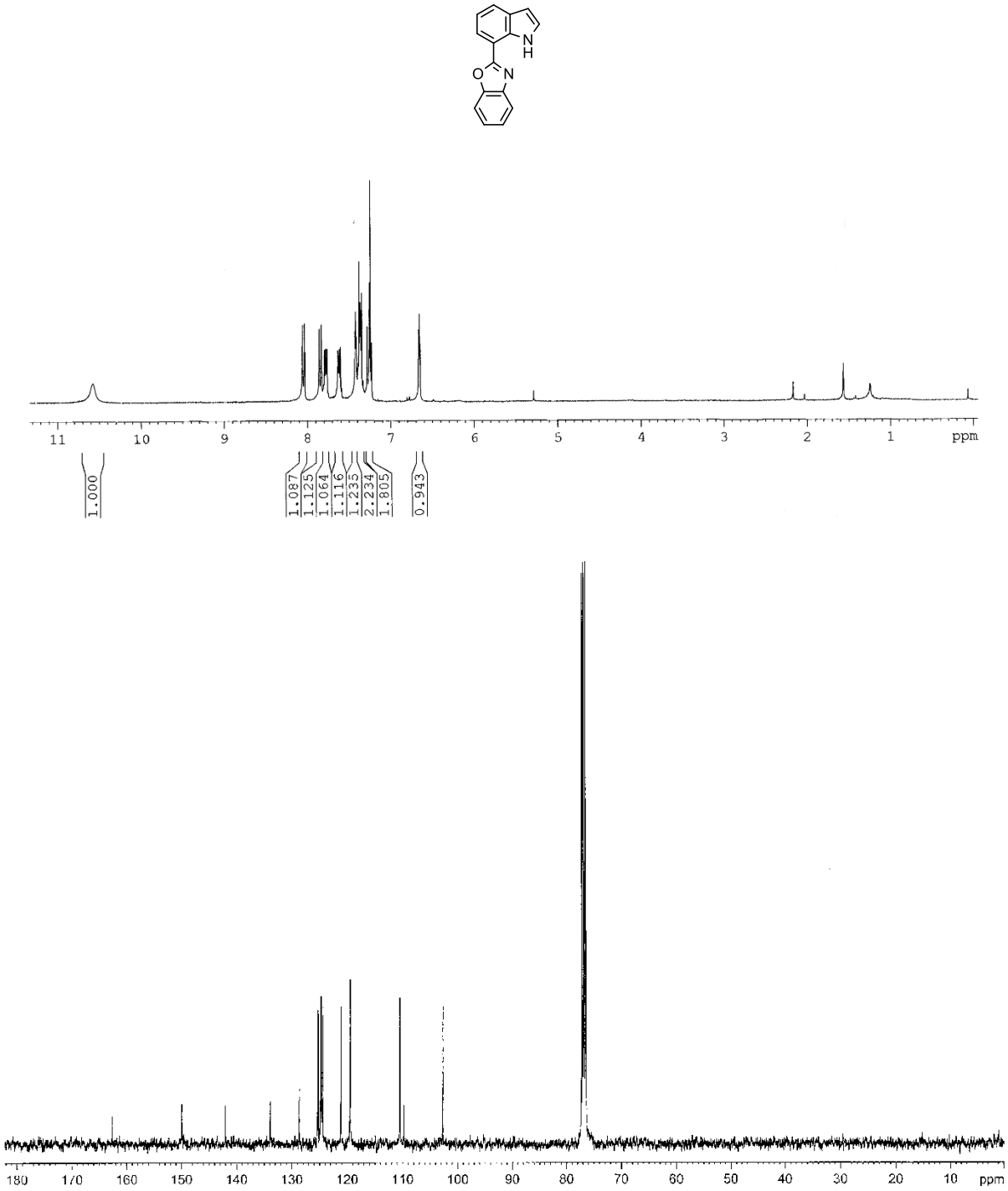

Figure S6. ^{1}H-NMR and ^{13}C-NMR spectra of compound **6**

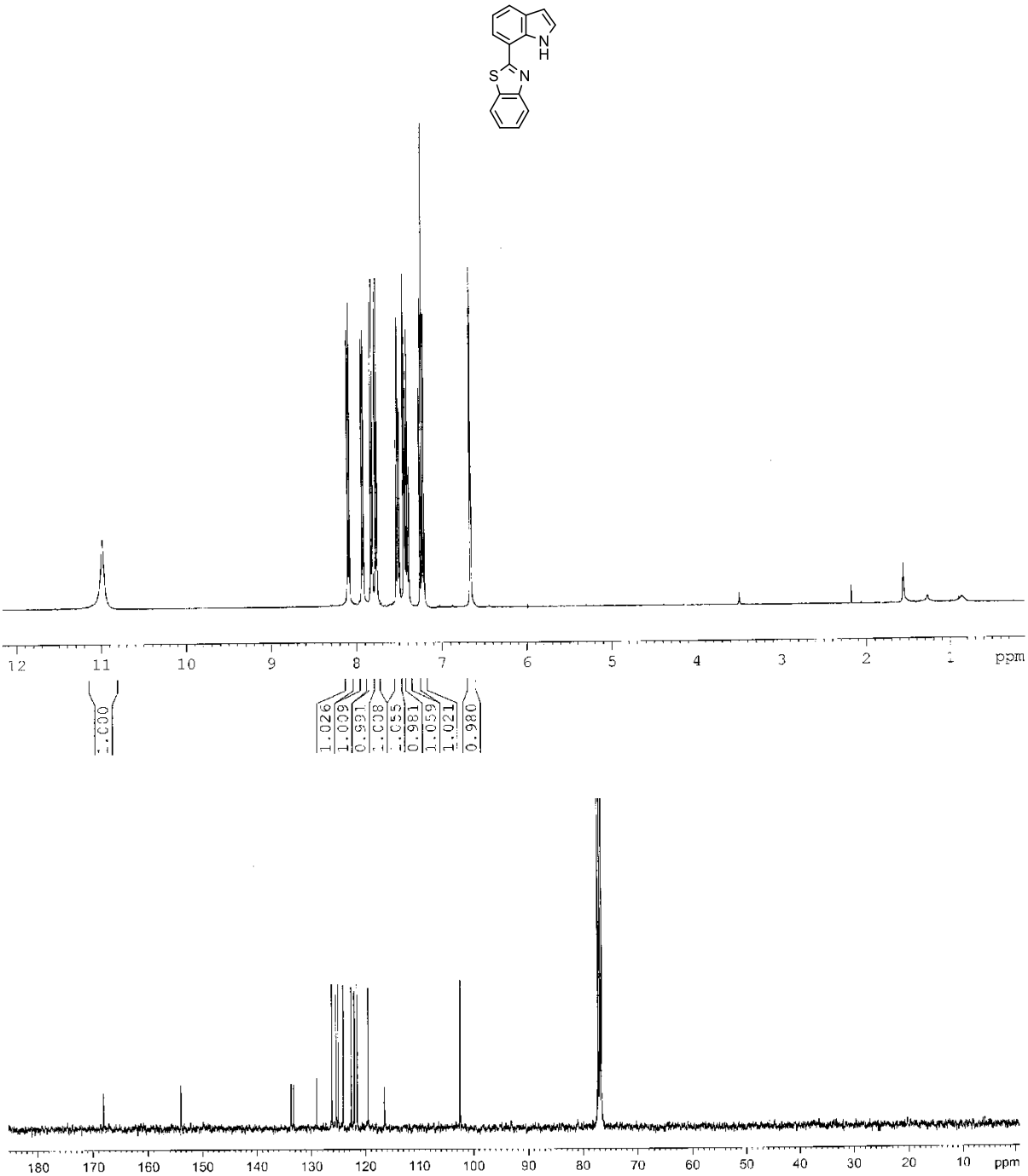

Figure S7. ^{1}H-NMR and ^{13}C-NMR spectra of compound **7**.

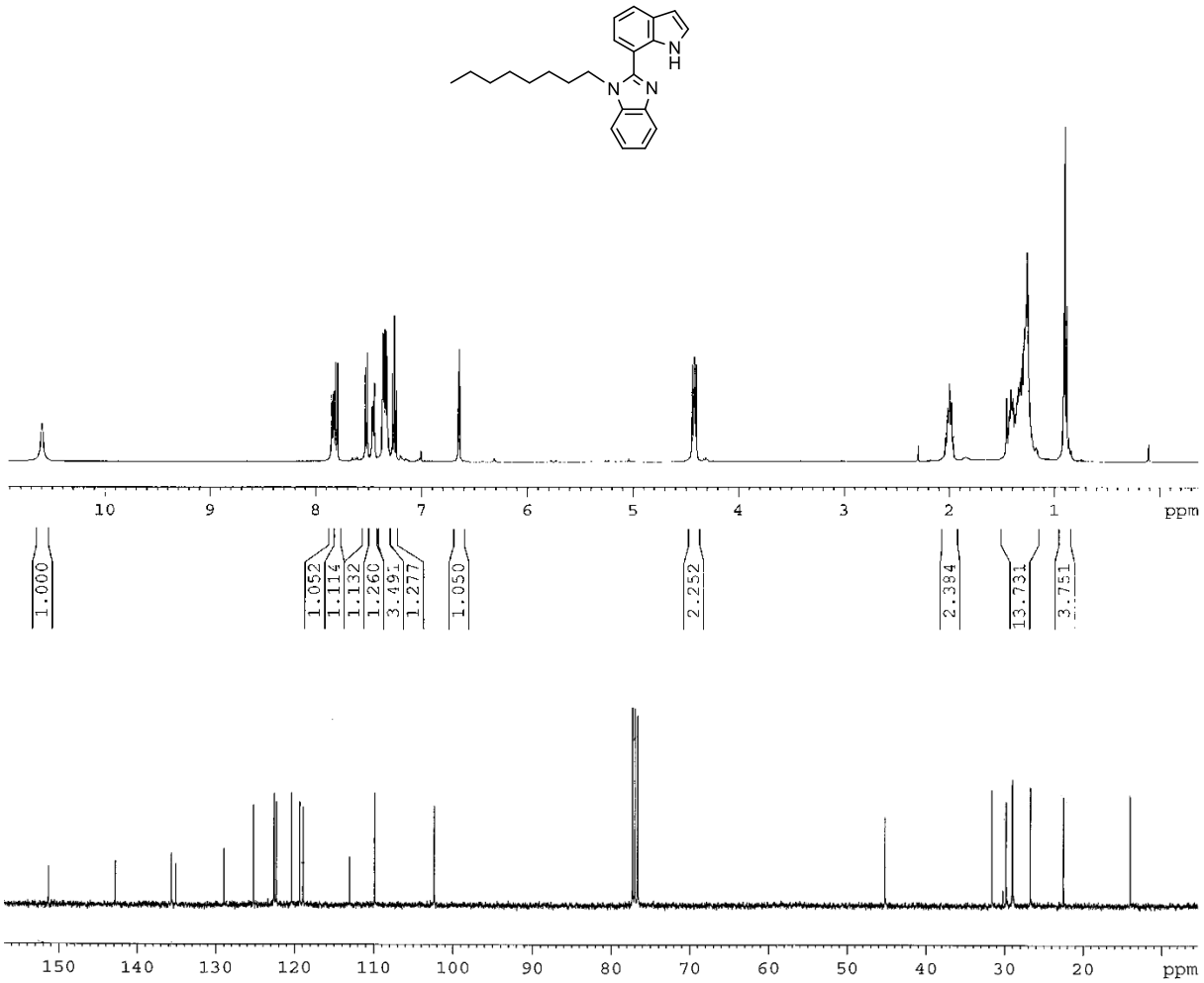

Figure S8. ^{1}H-NMR and ^{13}C-NMR spectra of compound **8**.

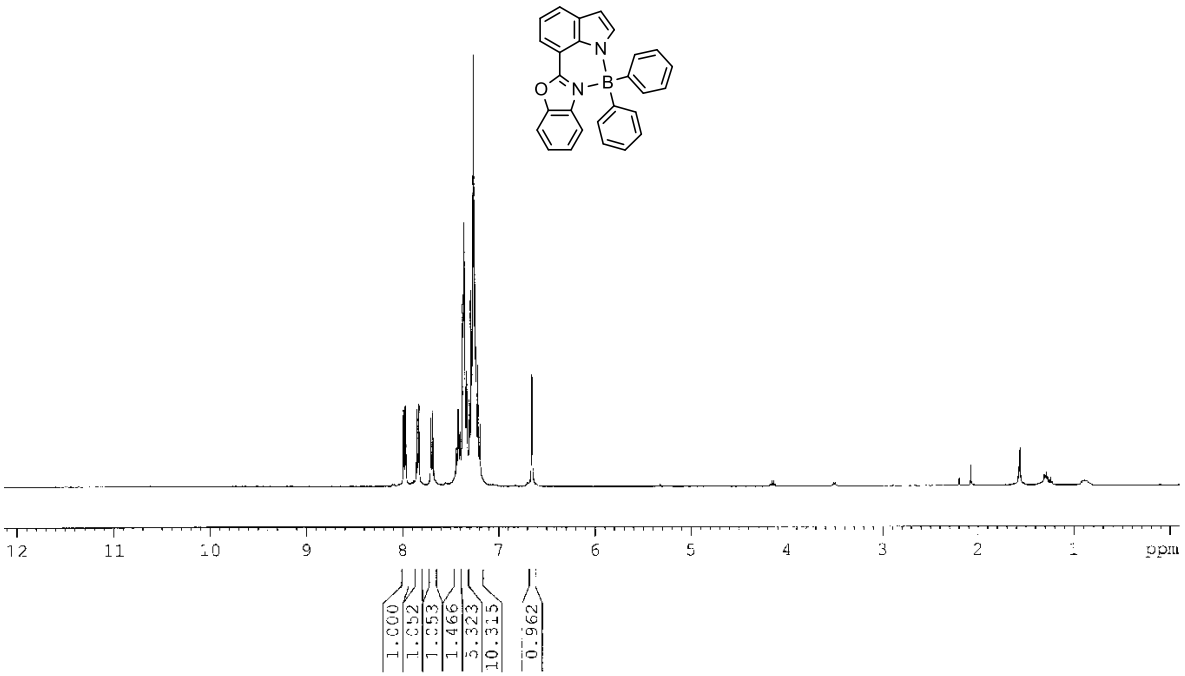

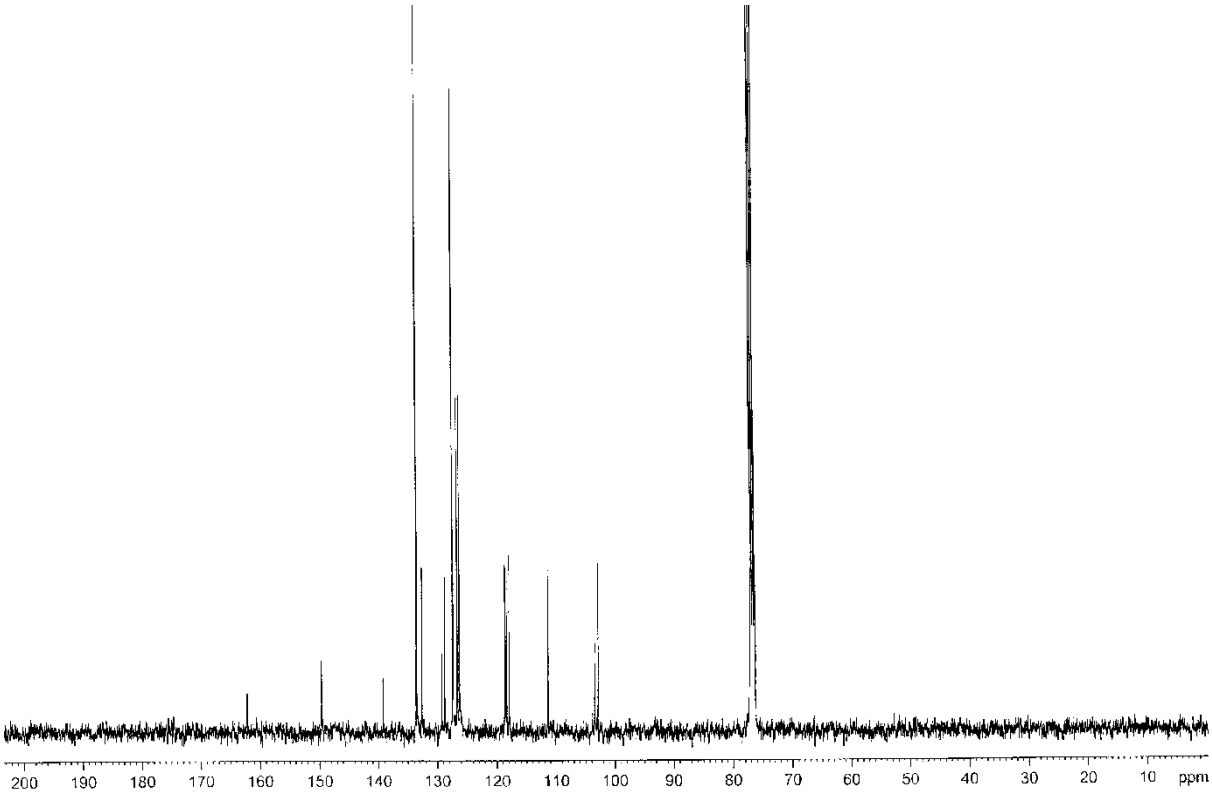

Figure S9. ^{1}H-NMR and ^{13}C-NMR spectra of compound **10**.

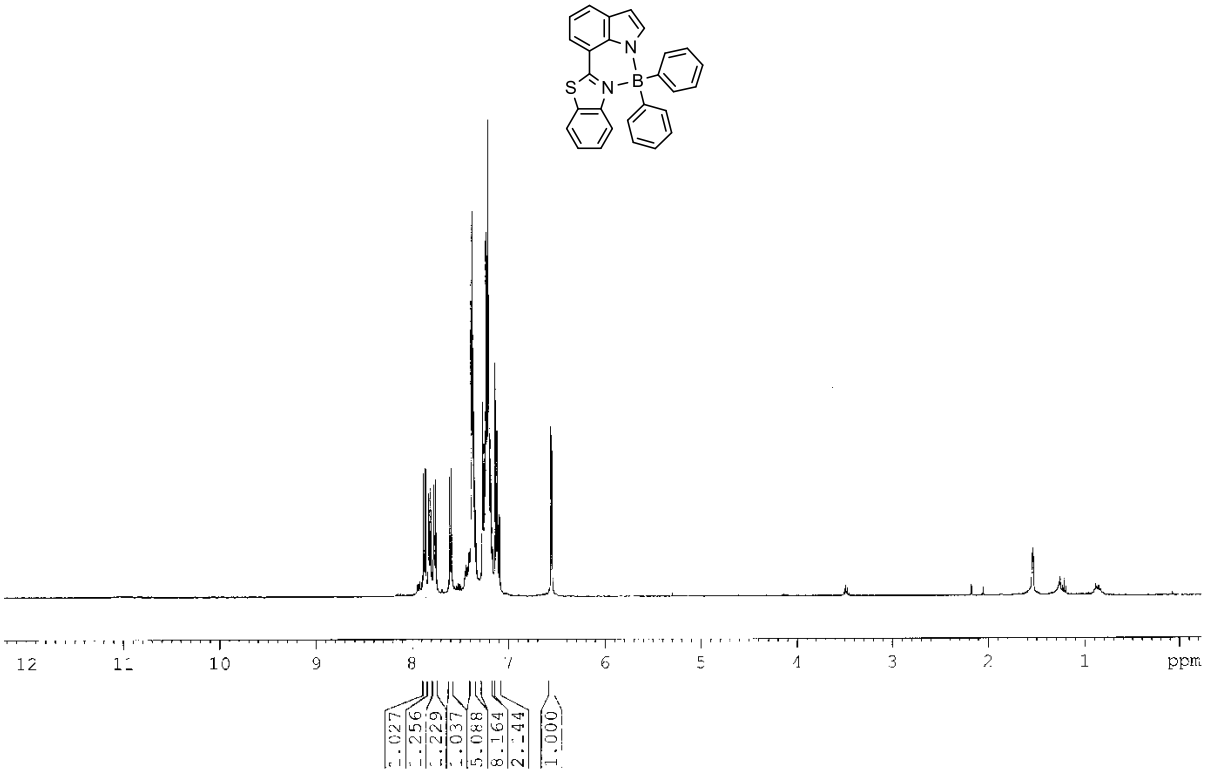

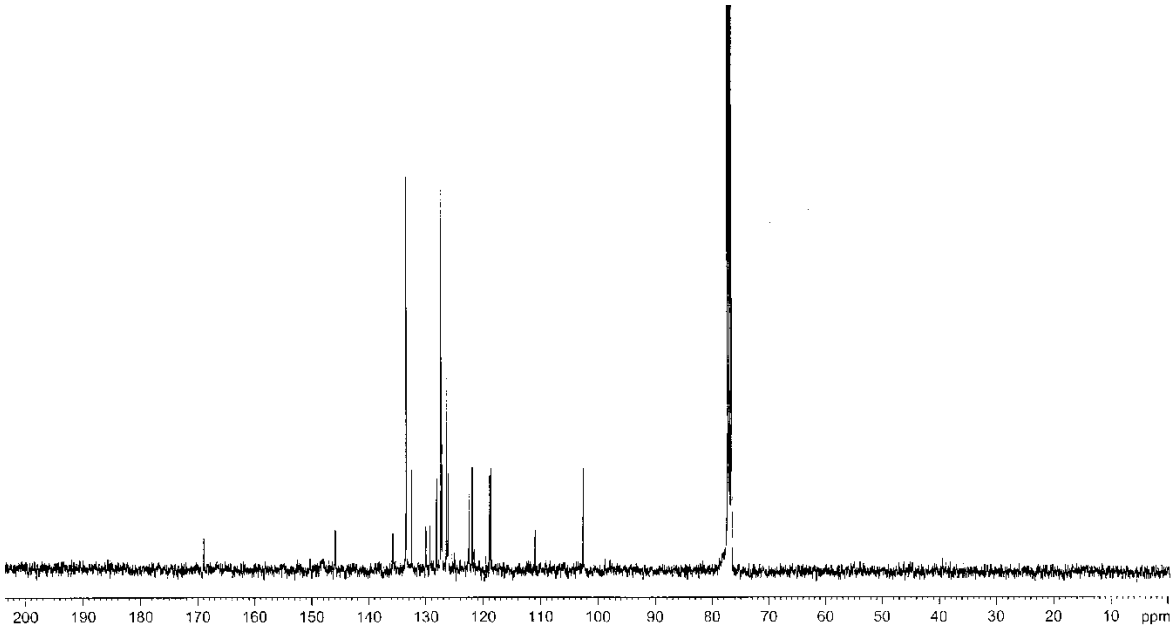

Figure S10. ^{1}H-NMR and ^{13}C-NMR spectra of compound **11**.

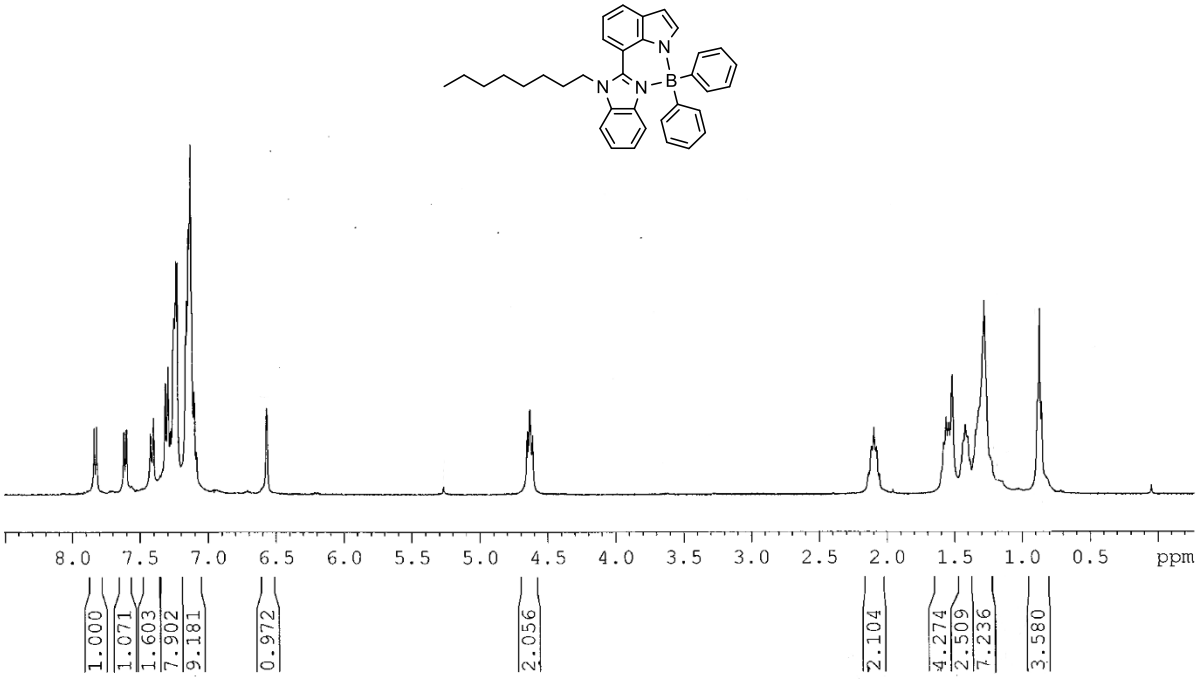

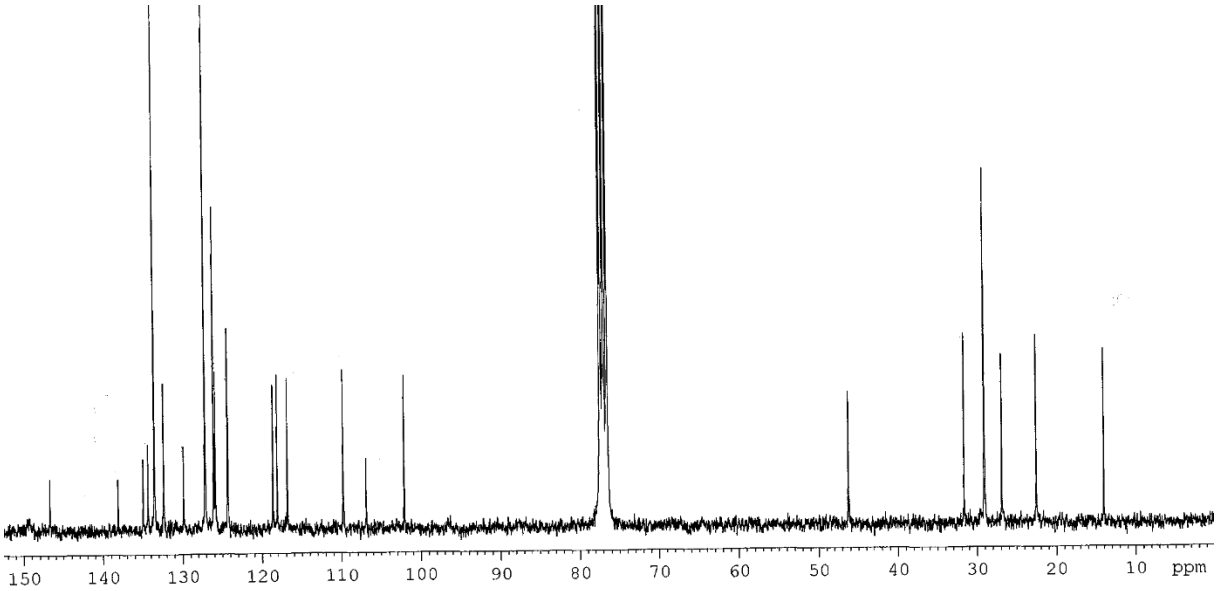

Figure S11. ^{1}H-NMR and ^{13}C-NMR spectra of compound **12**.

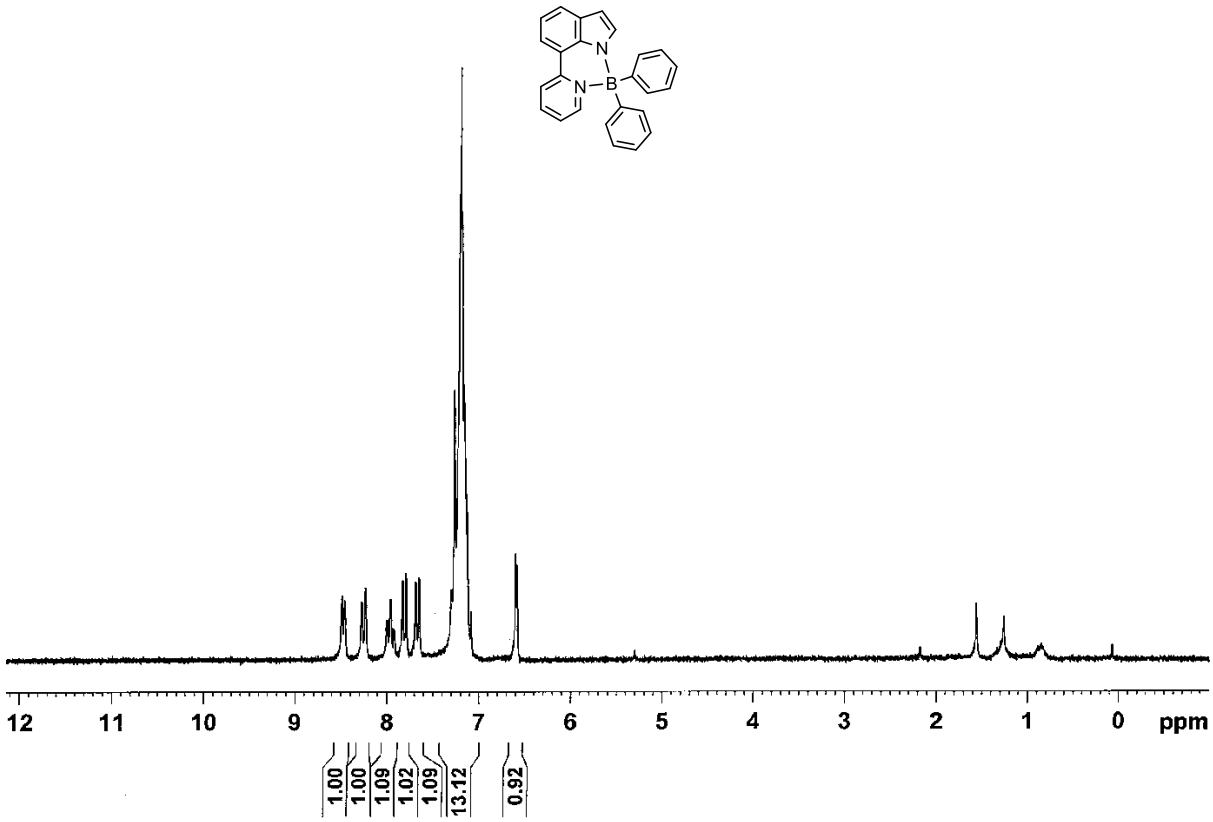

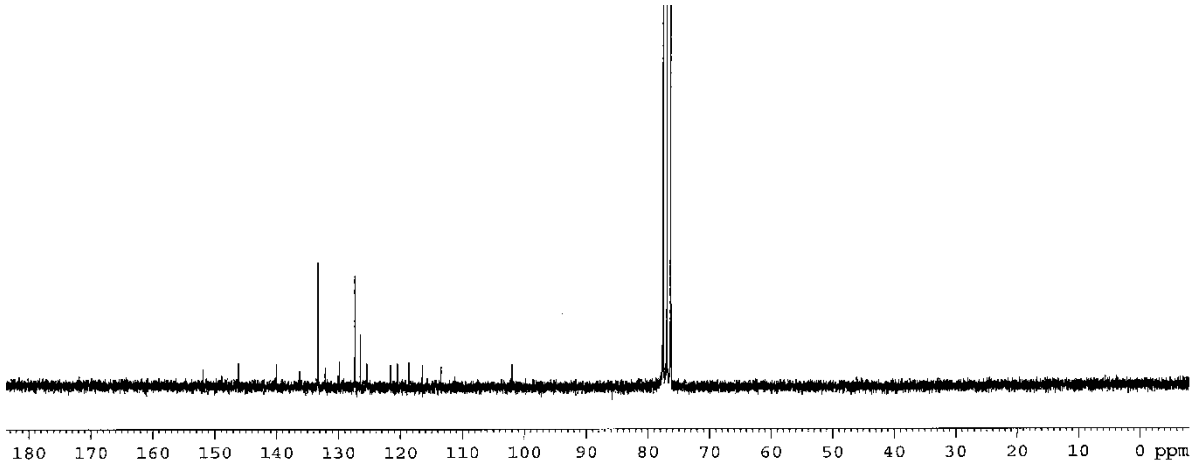

Figure S12. ^{1}H-NMR and ^{13}C-NMR spectra of compound **13**.

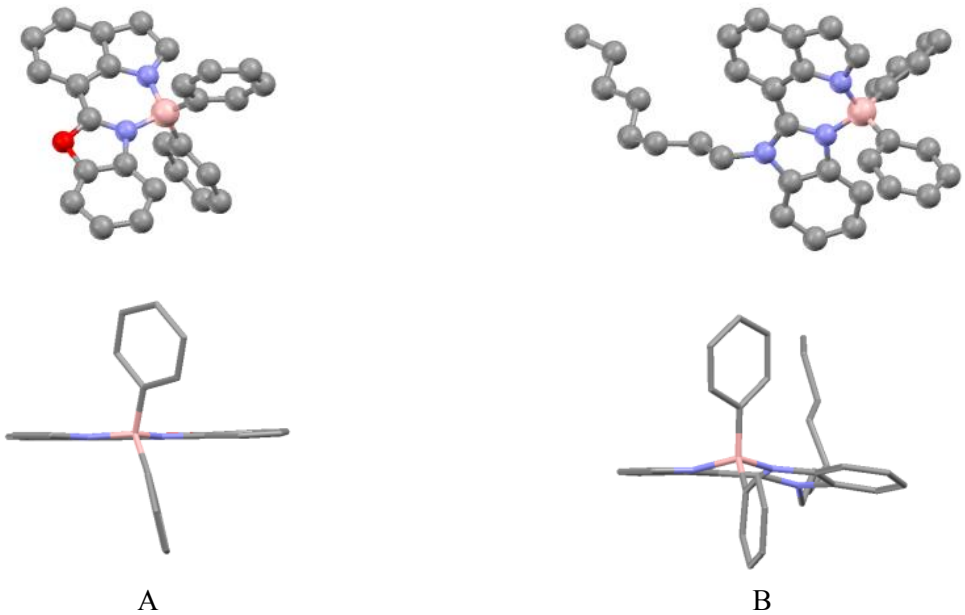

Figure S13. Crystal structures of compounds **10** (A) and **12** (B).

The complexation of boron generates a six-membered diazaboracycle where the boron center adopts a distorted tetrahedral geometry verified by the different bond angles measured for the N-B-N, C-B-C or N-B-C sequences. Differences in the bond lengths to the boron atom, were also observed. This was detected even for the C-B bonds between the boron atom and the chemically equivalent phenyl rings. The B-N_{indole} distance is very similar for both **10** and **12**. However, as expected from the different heteroaromatic component attached to the indole system, dissimilar bond distances are detected for the B-$N_{benzoxazole}$ and B-$N_{benzimidazole}$. It is also worth highlighting the good coplanarity observed for the extended π-conjugate system formed by the indole unit and the azaheteroaromatic component (Figure S13-A).

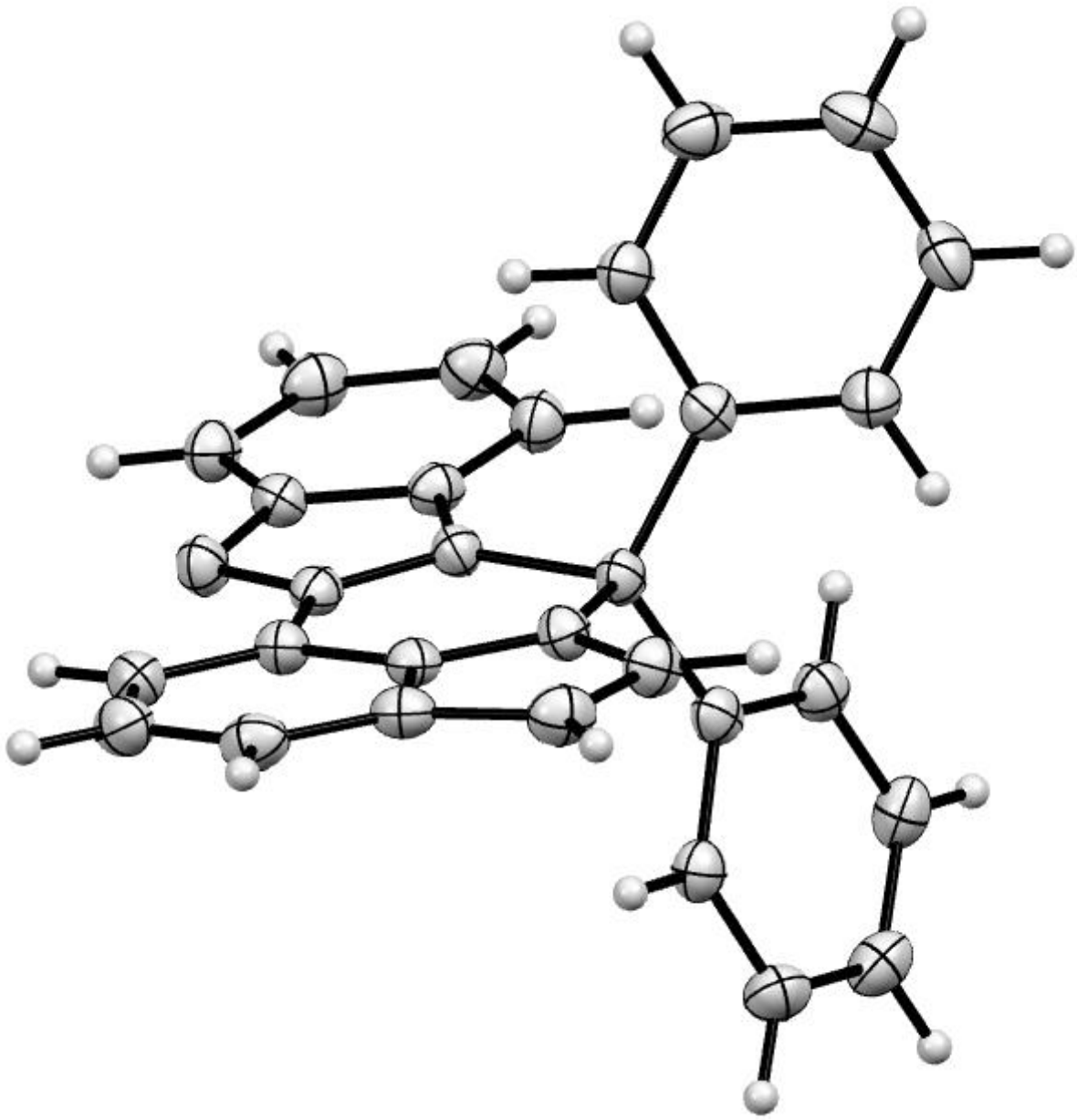

Figure S14. X-ray structure of compound **10** (thermal ellipsoid probability level: 50%).

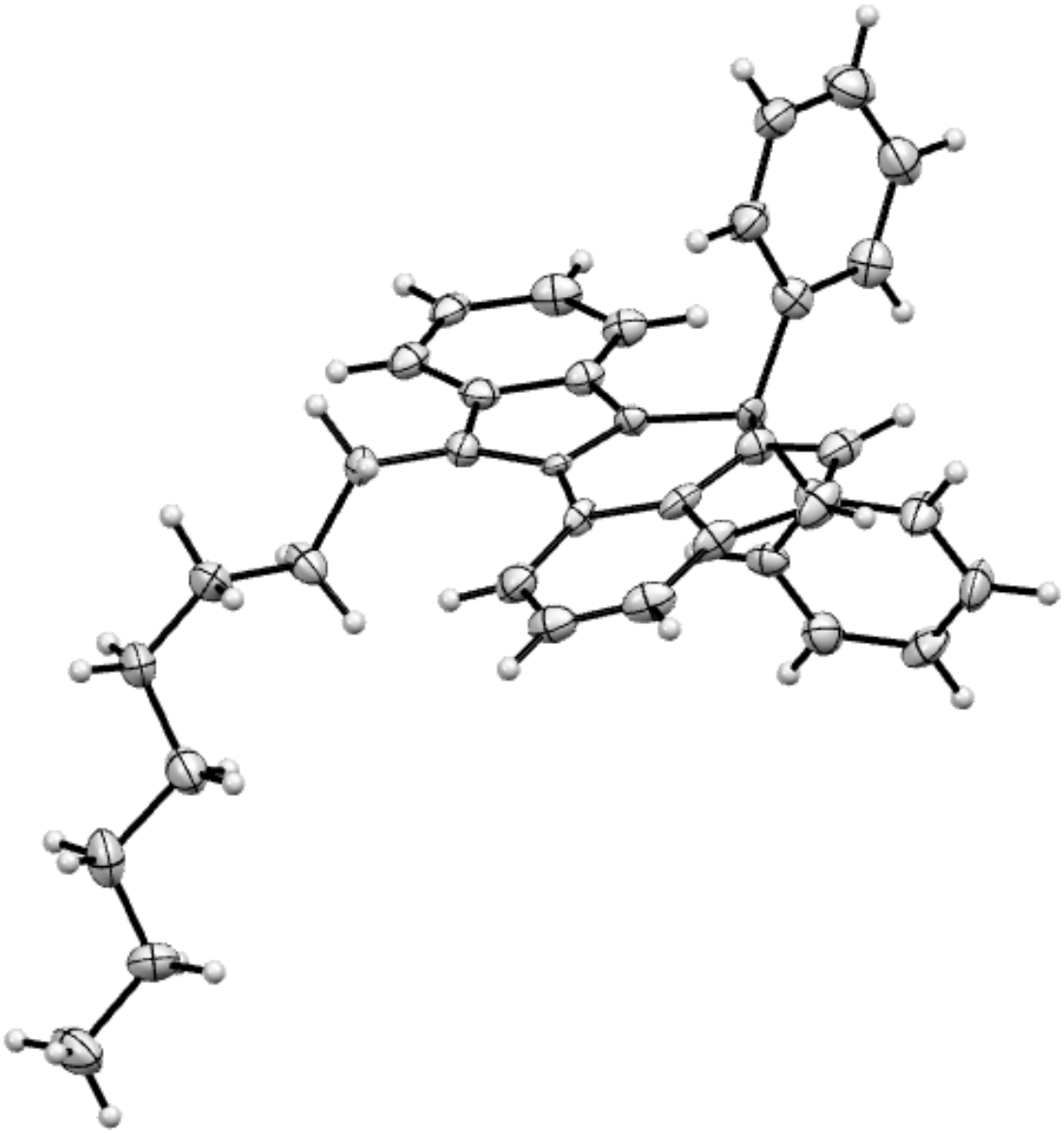

Figure S15. X-ray structure of compound **12** (thermal ellipsoid probability level: 50%).

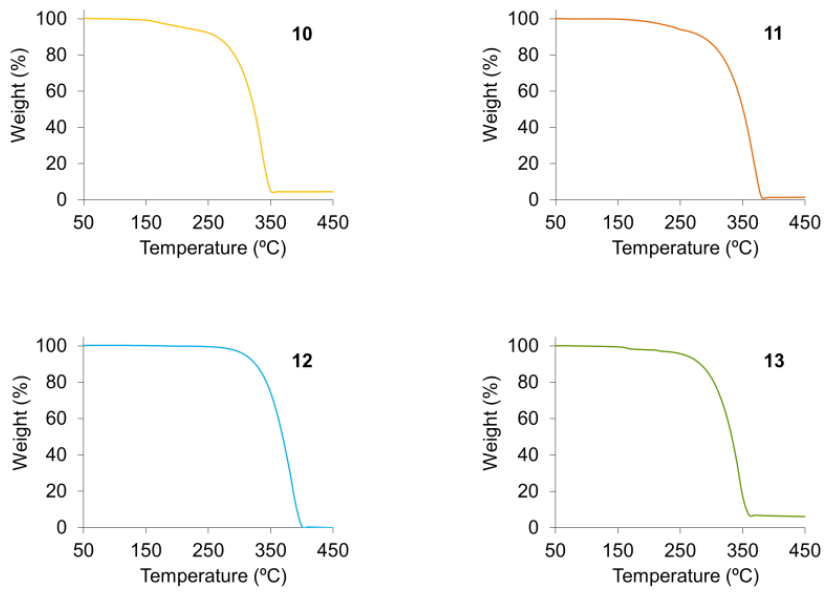

Figure S16. Thermogravimetric analysis of the boron complexes **10-13**.

Table S1. Decomposition temperature.

	10	**11**	**12**	**13**
T (ºC) (5% mass loss)	260	310	285	265

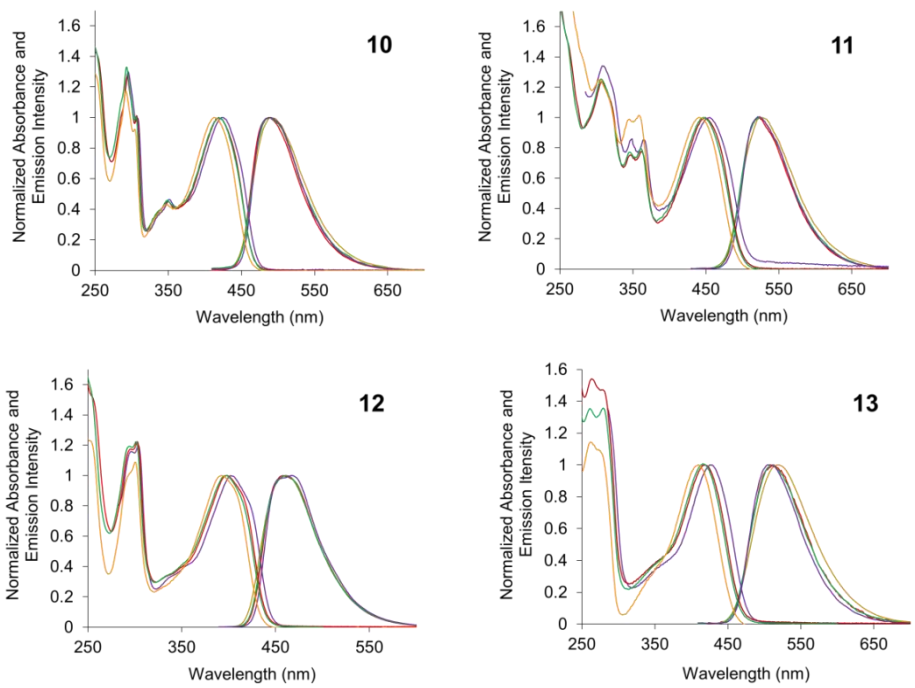

Figure S17. Solvent effects on the absorption and emission spectra of the boron complexes **10-13** in toluene (purple), dichloromethane (red), ethanol (green) and acetonitrile (yellow) ($2x10^{-5}$M).

Lippert-Mataga model: $\Delta\tilde{\nu} = \frac{(\mu_e-\mu_g)^2}{2\pi\varepsilon_0 hca^3}\left[\frac{\varepsilon-1}{2\varepsilon+1} - \frac{n^2-1}{2n^2+1}\right] + C$; $\Delta f = \left[\frac{\varepsilon-1}{2\varepsilon+1} - \frac{n^2-1}{2n^2+1}\right]$

$\Delta\tilde{\upsilon} = \tilde{\upsilon}_{abs.} - \tilde{\upsilon}_{em.}$: Stokes shift
μ_e : Dipole moment in the excited state.
μ_g : Dipole moment in the ground state.
ε_0: Vacuum permittivity.
h: Planck.s constant.
c: Speed of light.
a: Onsager radius
ε: Dielectric constant of the solvent.
n: Refraction index of the solvent.

Table S2. Stokes shifts of the boron complexes **10-13** in different solvents.

	$\tilde{\nu}_a - \tilde{\nu}_e$ (cm^{-1}) [$\lambda_e - \lambda_a$](nm)				*a (Å)*[a]
	Toluene	**CH_2Cl_2**	**EtOH**	**CH_3CN**	
10	3121 [65]	3374 [69]	3374 [69]	3804 [77]	5.40
11	2894 [69]	3077 [72]	3287 [77]	3751 [87]	5.34
12	3277 [61]	3291 [60]	3496 [64]	3753 [68]	8.67
13	3750 [81]	4296 [92]	4353 [92]	5182 [110]	4.50
Δf	0.013	0.217	0.289	0.305	

[a] Onsager radius estimated as half of the longest interatomic distance in the molecule, taken from the X-ray structure or the DFT molecular models.

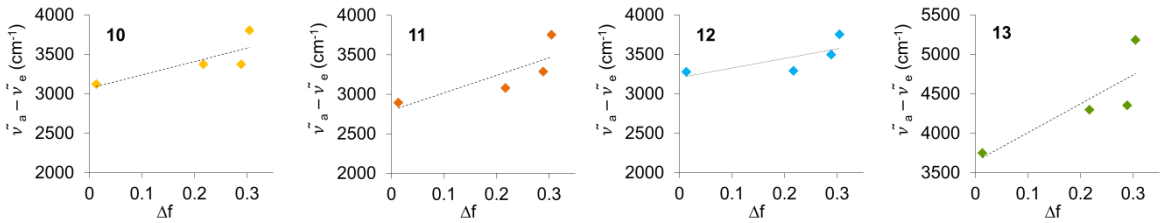

Figure S18. Lipert_Mataga plots of the boron complexes **10-13**.

Table S3. Variation between the ground state dipole moment and the excited state dipole moment of the boron complexes **10-13**.

	10	**11**	**12**	**13**
μ_e-μ_g (D)	0.58	0.89	0.58	0.51

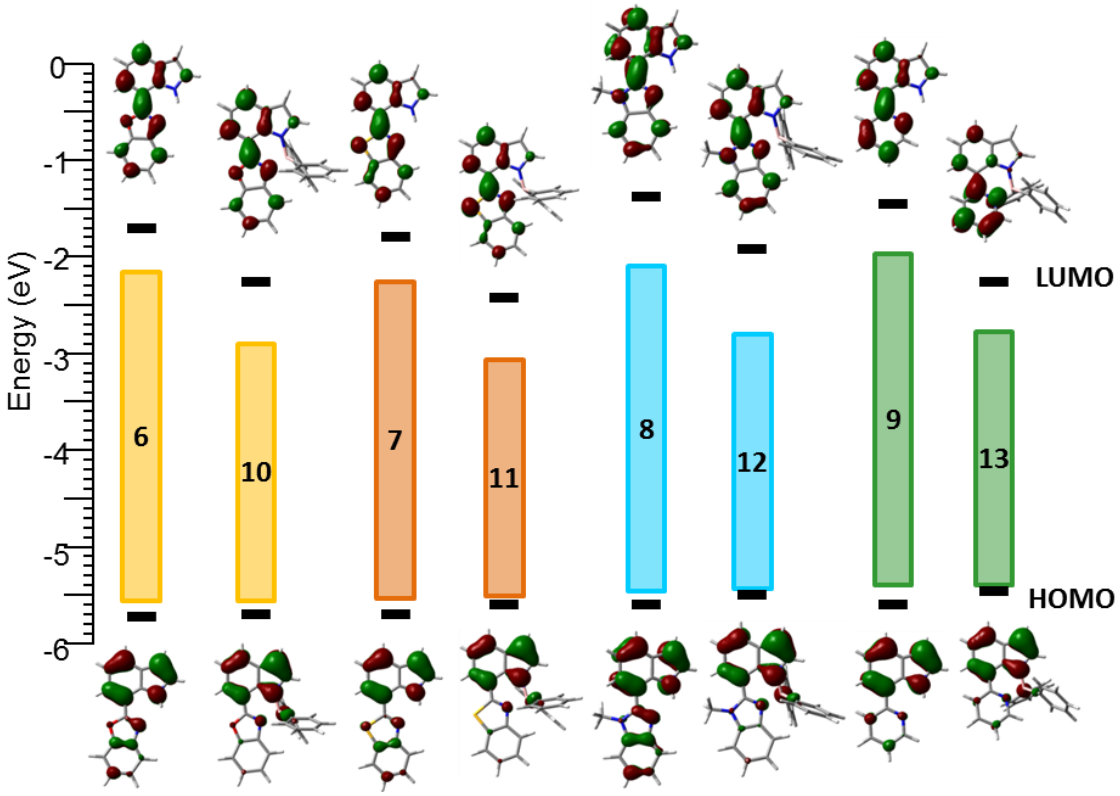

Figure S19. HOMO and LUMO energies (experimental: columns; theoretical: black dashes) and isosurfaces for the ligands **6-9** and boron complexes **10-13**.

Table S4. TD-DFT calculation of the absorption spectrum of compound **10**.

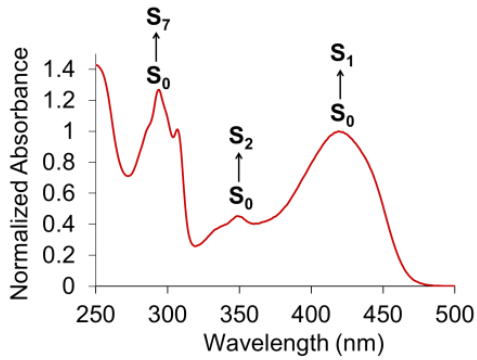

State	Wavelength (nm)	Oscillator Strength
1	429.1	0.204966093
2	368.9	0.062519353
3	363.0	0.006252426
4	348.8	0.027630075
5	352.3	0.015106536
6	347.7	0.000266778
7	285.6	0.326177583
8	279.8	0.020094757

State 1	Configuration Interaction
HOMO-6 → LUMO	0.021831
HOMO → LUMO	0.928658
State 2	
HOMO-1 → LUMO	0.940181
HOMO → LUMO+7	0.023649
State 7	
HOMO-7 → LUMO	0.047271
HOMO-7 → LUMO+2	0.014015
HOMO-6 → LUMO	0.773869
HOMO-3 → LUMO	0.017704
HOMO → LUMO	0.019562
HOMO → LUMO+1	0.036516
HOMO → LUMO+2	0.010667
HOMO → LUMO+4	0.013975
HOMO → LUMO+7	0.015668

	10
LUMO+1	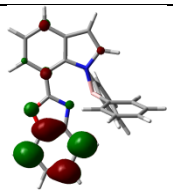
LUMO	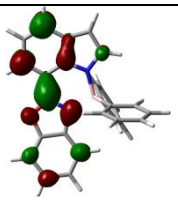
HOMO	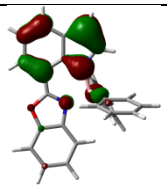
HOMO-1	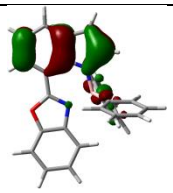
HOMO-2	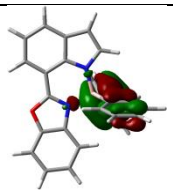
HOMO-3	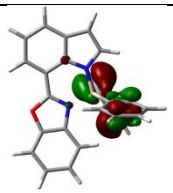
HOMO-4	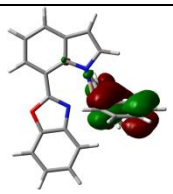
HOMO-5	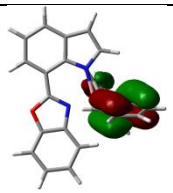
HOMO-6	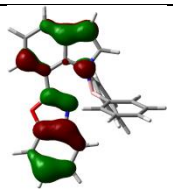

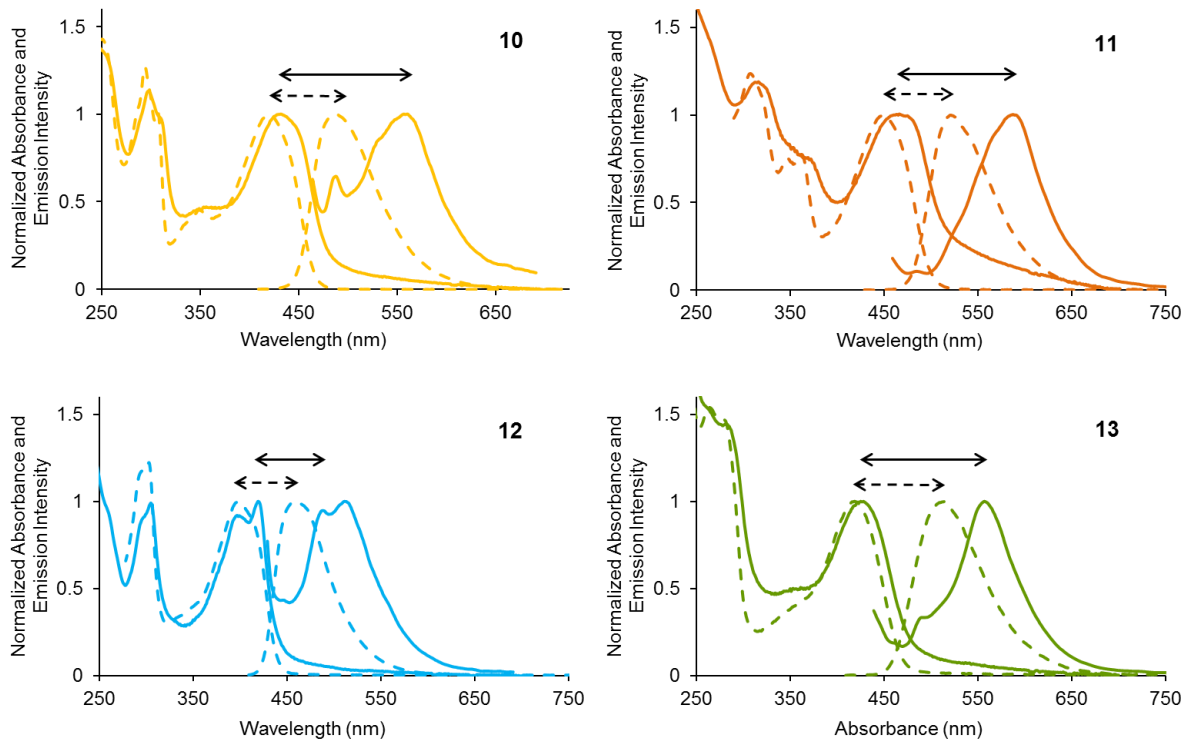

Figure S20. Absorption and emission spectra in solution (CH_2Cl_2, $2x10^{-5}$M, dashed plot) and in solid thin film (continuous plot) of the boron complexes.

Table S5. Stokes shift in solid thin films.

	10	**11**	**12**	**13**
λ_{em}-λ_{abs} (nm)	125	122	92	129

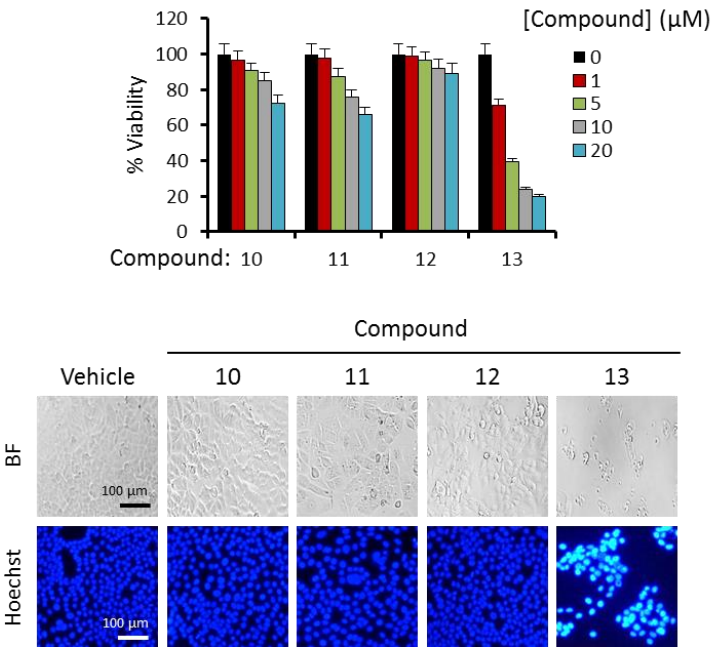

Figure S21. Effect of organoboron compounds **10-13** on the human breast cancer cell line MCF7. (a) Concentration-dependent effect on the viability of MCF7 treated during 48 h with indicated compounds. (b) Morphology of untreated MCF7 cells (vehicle) compared with those subjected to 48 h of treatment with 10 µM of indicated compounds. Morphology was determined by bright field (BF) microscopy. The Hoechst assay was used to asses apoptosis induction in untreated MCF7 cells (vehicle) and those cells subjected to 48 h of treatment with 10 µM of indicated compounds. Strong fluorescence was observed in the nuclei of apoptotic cells treated with compound **13**, while weak fluorescence was observed in other treatments corresponding to non-apoptotic cells.

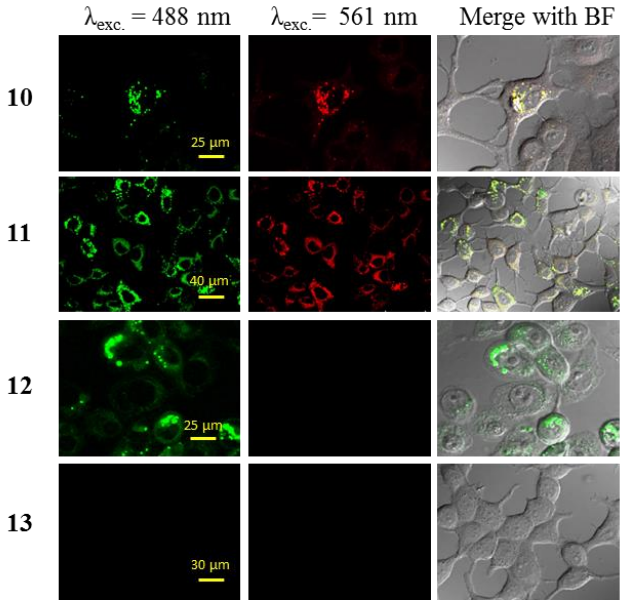

Figure S22. Confocal microscopy of compounds **10-13.**